LETTER

Vertical GaN junction barrier Schottky diodes with near-ideal performance using Mg implantation activated by ultra-high-pressure annealing

Applied Physics Express 15, 101004 (2022)
https://doi.org/10.35848/1882-0786/ac8f81

LETTER

Vertical GaN junction barrier Schottky diodes with near-ideal performance using Mg implantation activated by ultra-high-pressure annealing

Dolar Khachariya[1*], Shane Stein[2], Will Mecouch[1], M. Hayden Breckenridge[3], Shashwat Rathkanthiwar[3], Seiji Mita[1], Baxter Moody[1], Pramod Reddy[1], James Tweedie[1], Ronny Kirste[1], Kacper Sierakowski[4], Grzegorz Kamler[4], Michal Bockowski[4], Erhard Kohn[3], Spyridon Pavlidis[2], Ramón Collazo[3], and Zlatko Sitar[1,3]

[1]Adroit Materials, Inc., 2054 Kildaire Farm Rd., Cary, North Carolina 27539, United States of America
[2]Department of Electrical and Computer Engineering, North Carolina State University, Raleigh, North Carolina 27695, United States of America
[3]Department of Materials Science and Engineering, North Carolina State University, Raleigh, North Carolina 27695, United States of America
[4]Institute of High-Pressure Physics, Polish Academy of Sciences, Sokołowska 29/37, 01-142 Warsaw, Poland

*E-mail: dkhacha@ncsu.edu

Received August 19, 2022; revised August 23, 2022; accepted September 4, 2022; published online September 23, 2022

We report a kV class, low ON-resistance, vertical GaN junction barrier Schottky (JBS) diode with selective-area p-regions formed via Mg implantation followed by high-temperature, ultra-high pressure (UHP) post-implantation activation anneal. The JBS has an ideality factor of 1.03, a turn-on voltage of 0.75 V, and a specific differential ON-resistance of 0.6 mΩ·cm^2. The breakdown voltage of the JBS diode is 915 V, corresponding to a maximum electric field of 3.3 MV cm^{-1}. These results underline that high-performance GaN JBS can be realized using Mg implantation and high-temperature UHP post-activation anneal. © 2022 The Japan Society of Applied Physics

GaN is poised to be the material of choice for kV-class power electronics due to its wide bandgap, high saturation velocity, and high critical electric field.[1,2] In comparison to planar GaN power devices, vertical GaN devices are capable of achieving higher breakdown voltages and current levels with smaller chip areas while also benefitting from the high thermal conductivity of the bulk substrates and thus a superior thermal management.[1,2]

Due to their low turn-on voltage and fast switching speed, the Schottky diodes are attractive for high-power applications. However, they suffer from a high electric field near the surface metal contact, which increases the leakage current and reduces the breakdown voltage. In the p–n diode, the peak of the electric field is, in contrast, pushed into the bulk, which provides ideal avalanche breakdown behavior, but at the cost of a higher turn-on voltage. Ideally, the junction barrier Schottky (JBS) diode should combine the low turn-on voltage and ON-resistance properties of a Schottky barrier diode and towards avalanche breakdown characteristics of the p–n junction diode.

A major technological hurdle for vertical GaN JBS diodes is selective area p-type doping. As in Si and SiC, ion implantation is the preferred method for achieving this selectivity. However, activating the implanted Mg needs high temperatures that often results in surface deterioration due to GaN decomposition. To address this issue, several annealing techniques have been investigated.[3–8] Using a symmetrical multi-cycle rapid thermal annealing (SMRTA) process with a sputtered AlN capping layer, Zhang et al. reported vertical GaN JBS with R_{ON} of 1.7 mΩ·cm^2 and BV of 600 V.[9] Recently, Zhou et al. demonstrated quasi-vertical GaN JBS diodes with R_{ON} of 2.75 mΩ·cm^2 and BV of 838 V using single-step annealing with a SiO_2 capping layer.[10] Compared to these annealing approaches, the ultra-high pressure annealing (UHPA) technique not only avoids the use of a capping layer but also enables superior Mg activation efficiency.[11–15] However, its implementation in JBS diodes has not been demonstrated.

In this work, we report on high-performance vertical GaN JBS diodes using the UHPA technique. The JBS diode still shows typical Schottky barrier characteristics in forward bias exhibiting record-low ON-resistance in combination with excellent material quality. On the other hand, the JBS diode showed a record-high breakdown voltage, identical to the p–n junction on the same wafer. No noticeable degradation was observed in the monolithic integration of both Schottky and p–n device architectures on the identical material.

A 5 μm thick n$^-$-GaN epilayer was grown using a vertical, cold-wall, radio frequency (RF) heated, low-pressure metalorganic chemical vapor deposition (MOCVD) reactor on an ammonothermal n$^+$-GaN substrate.[16] Details of the growth conditions can be found elsewhere.[17] The net carrier concentration (N_D–N_A) of the n$^-$-GaN drift layer was extracted to be $\sim 1.3 \times 10^{16}$ cm^{-3} using capacitance–voltage (C–V) measurements at 1 MHz.[18] To achieve a shallow box profile (~100 nm) of implanted Mg at a concentration of $\sim 2 \times 10^{19}$ cm^{-3}, a two-step implantation process with ion energies of 75 keV and 25 keV and corresponding doses of 2×10^{14} cm^{-2} and 4.4×10^{13} cm^{-2}, respectively, were used with a tilt angle of 7°. After the implantation, activation annealing was performed at 1300 °C for 30 min at a high pressure of 400 MPa in a N_2 ambient to prevent decomposition.[11] A detailed investigation on p-type GaN formed via Mg implantation and UHPA post-implantation has been reported in our earlier work.[11] The activation anneal condition chosen in this work corresponds to the diffusion budget of around 0.36, resulting in high Mg activation.[11]

The device fabrication involved e-beam evaporation of Ni/Au-based p-type Ohmic contact followed by a contact anneal at 600 °C for 10 min in air ambient. Then, Ni/Au-based Schottky contacts were deposited. Finally, a Ti/Al/Ni/Au Ohmic metal stack was deposited on the back side of the n$^+$−GaN substrate. In addition to the JBS diodes, Schottky diodes with and without edge terminations (ET) and p–n diodes were fabricated on the same wafer for comparison. Figures 1(a) and 1(b) show the schematic cross-section of the fabricated Schottky diode with Mg implanted p-GaN ET and JBS diode, respectively. For the JBS diode, the widths of the p-GaN (W_P) and n$^-$-GaN (W_N) regions were designed to be 3 and 4 μm, respectively. The device area was 0.1 × 0.1 mm^2.

Figure 2(a) shows the room temperature current–voltage (I–V) characteristics comparison of the vertical Schottky with

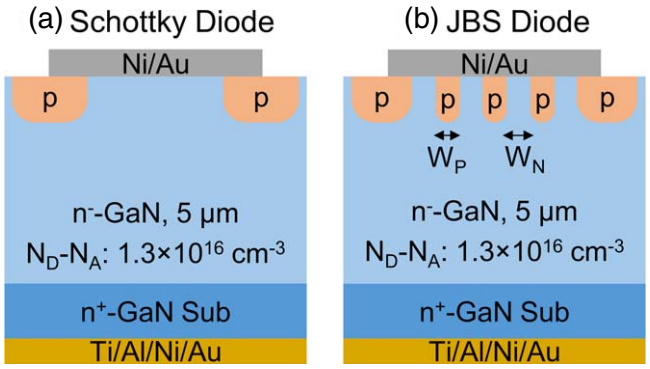

Fig. 1. (Color online) A schematic cross-section of the (a) reference Schottky diode with Mg implanted p-GaN edge termination and (b) JBS diode. For the JBS diode, the width of p-GaN (W_P) is 3 μm, and n$^-$-GaN (W_N) is 4 μm.

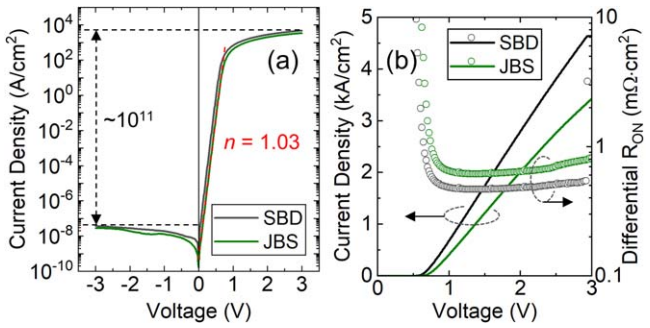

Fig. 2. (Color online) (a) Comparison of room temperature *I*–*V* characteristics of the Schottky barrier and JBS diode in semi-log scale. (b) *I*–*V* comparison of the Schottky barrier and JBS diode in linear scale (left *y*-axis) and the differential R_{ON} for both diodes in semi-log scale (right *y*-axis).

ET and JBS diode for ±3 V in a semi-log scale. The ideality factor (n) for both diodes is 1.03, which indicates near-ideal Schottky behavior. As per the graph, the rectification ratios (I_{ON}/I_{OFF}) at ±3 V for both diodes are $\sim 10^{11}$. These results indicate that high-quality Schottky contacts can be realized even after high-temperature anneal, and thus the surface characteristics are preserved during high-temperature activation anneal with the help of N_2 overpressure. Figure 2(b) shows the *I*–*V* characteristics for both diodes on a linear scale. The turn-on voltage (V_{ON}) for the Schottky diode and JBS diode is 0.7 V and 0.75 V, respectively. As seen in these graphs, the similarity of *I*–*V* in Schottky and JBS diodes indicates that the Schottky contact dominates the forward characteristics of the JBS.

The differential ON-resistance (R_{ON}) reflects the material's properties of the Schottky diode part, which has not degraded during the high-temperature annealing and activation process. The R_{ON} for both diodes is also shown in Fig. 2(b). The extracted R_{ON} for the Schottky diode is 0.46 mΩ·cm^2. The specific R_{ON} of the GaN substrate is 0.22 mΩ·cm^2, calculated using the resistivity measured via a 4-point probe (6 mΩ·cm) and the wafer thickness (370 μm). Thus, the specific R_{ON} of the n$^-$-GaN drift layer is 0.24 mΩ·cm^2. The electron mobility in the drift layer can be estimated using the R_{ON} and doping of the n$^-$-GaN. The calculated electron mobility for the drift layer is $\sim$1000 cm^2 V·s^{-1}, which aligns with our previous results.[17] This confirms the high-quality GaN epilayer used here as a drift layer. In comparison, the differential R_{ON} for the JBS diode is 0.6 mΩ·cm^2, which is only 0.14 mΩ·cm^2 (30%) higher than the Schottky diode. The ON-resistance of our JBS diode is the lowest value amongst all GaN-based JBS reported in the literature.[9,10] Moreover, the extracted R_{ON} of the JBS diode also includes the substrate resistance, which is 36% of the total resistance of the JBS diode. Thus, removing or thinning the GaN substrate would further reduce the R_{ON}. Based on the current flow path from anode to cathode, the R_{ON} for the JBS diode can be modeled by distributing the total resistance into three components in addition to the substrate resistance: channel resistance, current spreading resistance, and remaining drift layer resistance.[19,20] It is worth noting that the extracted R_{ON} of the JBS diode from experimental results matches precisely the modeled R_{ON}.[20]

Figure 3(a) shows the reverse bias *I*–*V* comparison between the Schottky diodes with and without ET, JBS, and p–n diodes. As seen in the graph, the current compliance for all diodes is set at 1 A cm^{-2}. The Schottky diode without any ET breaks down at only 300 V. In comparison, the Schottky diode with Mg implanted p-type ET shows a breakdown of 500 V. The results suggest that the p-type ET reduces the electric field crowding at the Schottky metal edge, thus reducing the leakage current while increasing the breakdown capability. Compared to the Schottky diodes, the leakage current in the JBS diode increases very slowly. It is worth noting that the leakage current of the JBS diode at −500 V is still ~4 orders of magnitude lower than the Schottky diodes. In the JBS diode, at relatively low reverse bias, the p-GaN regions deplete the lateral n$^-$-GaN channel region. At high reverse bias, the maximum E-field is now developed across the p–n interface; thus, the p-GaN regions shield the Schottky interface of the JBS from the high E-field.[19] As a result, the E-field at the Schottky interface of the JBS remains very low at high reverse bias, in turn

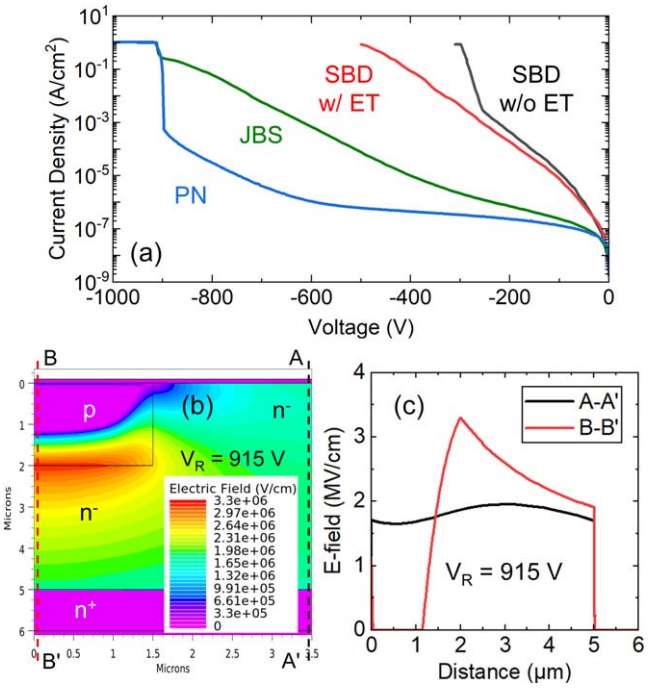

Fig. 3. (Color online) (a) Reverse bias *I*–*V* characteristics comparison between Schottky without and with edge termination (ET), JBS, and p–n diodes. (b) Simulated 2D electric field distribution in the unit cell of the JBS diode at reverse bias 915 V. (c) The E-field profile at the Schottky region of the JBS [dashed line A–A′ in (b)] and at the p–n junction interface of the JBS [dashed line B–B′ in (b)] at a reverse bias 915 V.

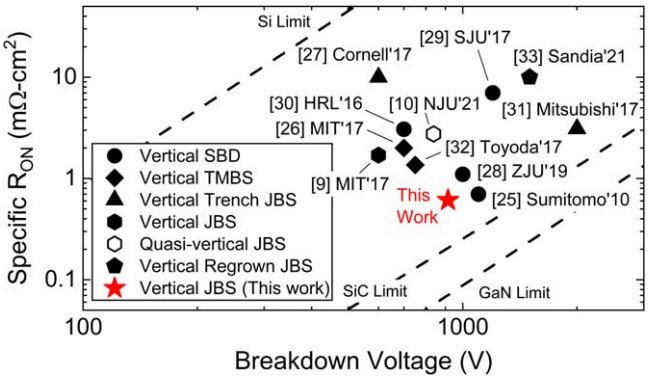

Fig. 4. (Color online) The specific R_{ON} versus breakdown voltage performance comparison of experimentally reported GaN Schottky and JBS diodes. Closed symbols represent vertical GaN-on-GaN diodes, and open symbols represent quasi-vertical diodes.

reducing the reverse bias leakage of the JBS diode compared to the Schottky diode. As shown in Fig. 3(a), the breakdown voltage of the JBS diode is 915 V, which is the highest BV reported value for GaN JBS in the literature. In comparison, the p–n diode with implanted p-GaN also shows a breakdown of 915 V. In contrast to the p–n diode, the JBS diode has slightly higher leakage.[21–23)] As seen in the graph, the reverse leakage current in the p–n diode is almost constant with respect to the reverse bias from 0 V to 600 V. Above 600 V, the leakage current increases approx. linearly with reverse bias in the semilogarithmic scale. For the JBS diode, the onset of the strong field dependence already appears at around 300 V, however, with a similar *I*–*V* slope as observed in the p–n diode at high reverse bias voltages. It can be speculated that this leakage is related to defects.

During the high-temperature activation process, the Mg ions diffuse and form a diffusion tail into GaN.[11)] Thus, in simulations, the p-type doping profile was modeled with the diffused Mg profile based on the diffusion budget estimated from earlier work.[11,24)] Figure 3(b) shows the simulated 2D electric field contour in a JBS unit cell at a reverse bias of 915 V. The maximum E-field in the JBS diode is across the p–n junction interface rather than at the Schottky interface. Figure 3(c) shows the E-field profile in the *y*-direction at the Schottky interface (A–A′) and p–n junction interface (B–B′). The maximum E-field in the JBS diode, at 915 V, is 3.3 MV cm^{-1} at the p–n junction interface, whereas the E-field at the Schottky metal interface is less than 2 MV cm^{-1}. It is thus evident that the selectively doped p-type regions in the JBS diode shield the Schottky surface from a higher E-field. However, the model does not include the impact of defects yet.

The performance of our vertical GaN JBS diode is benchmarked against other state-of-the-art GaN JBS and Schottky diodes reported in the literature using R_{ON} versus breakdown voltage graph as shown in Fig. 4.[9,10,25–33)] As seen in the graph, the JBS diodes presented in this work have high breakdown voltage (915 V) and very low ON-resistance (0.6 mΩ·cm^2) compared to the reported literature. These correlate to a state-of-the-art figure of merit value of 1.4 GW cm^{-2}.

In summary, we have reported record-performance vertical GaN JBS diodes using Mg implantation and UHPA activation. The near-unity ideality factor (n = 1.03) confirms that high-quality Schottky contacts can be formed following UHPA. Crucially, the devices exhibited record-low R_{ON} and record-high breakdown voltage of 0.6 mΩ·cm^2 and 915 V, respectively. We found no noticeable degradation due to the monolithic integration, including the high-temperature processes, of both Schottky and p–n diode architectures on the identical material.

Acknowledgments The authors gratefully acknowledge funding in part from NSF (ECCS-1916800, ECCS-1508854, ECCS-1610992, DMR-1508191, ECCS-1653383), DOE (DE-AR0000873, DE-AR000149), ONRG NICOP (N62909-17-1-2004), NCBR (TECHMATSTRATEG-III/0003/2019-00), and NCSU faculty start-up fund.

ORCID iDs Dolar Khachariya https://orcid.org/0000-0002-8780-4583 Shashwat Rathkanthiwar https://orcid.org/0000-0003-0180-1398

1) H. Amano et al., J. Phys. D: Appl. Phys. **51**, 163001 (2018).
2) J. Y. Tsao et al., Adv. Electron. Mater. **4**, 1600501 (2018).
3) T. J. Anderson, B. N. Feigelson, F. J. Kub, M. J. Tadjer, K. D. Hobart, M. A. Mastro, J. K. Hite, and C. R. Eddy Jr., Electron. Lett. **50**, 197 (2014).
4) M. J. Tadjer, B. N. Feigelson, J. D. Greenlee, J. A. Freitas, T. J. Anderson, J. K. Hite, L. Ruppalt, C. R. Eddy, K. D. Hobart, and F. J. Kub, ECS J. Solid State Sci. Technol. **5**, P124 (2016).
5) S. R. Aid, T. Uneme, N. Wakabayashi, K. Yamazaki, A. Uedono, and S. Matsumoto, Phys. Status Solidi A **214**, 1700225 (2017).
6) Y.-T. Shi et al., Sci. Rep. **9**, 8796 (2019).
7) V. Meyers et al., J. Appl. Phys. **128**, 085701 (2020).
8) I. C. Kizilyalli and E. P. Carlson, ECS Trans. **104**, 3 (2021).
9) Y. Zhang et al., IEEE Electron Device Lett. **38**, 1097 (2017).
10) F. Zhou, W. Xu, F. Ren, D. Zhou, D. Chen, R. Zhang, Y. Zheng, T. Zhu, and H. Lu, IEEE Electron Device Lett. **42**, 974 (2021).
11) M. H. Breckenridge et al., Appl. Phys. Lett. **118**, 022101 (2021).
12) H. Sakurai et al., Appl. Phys. Lett. **115**, 142104 (2019).
13) K. Sierakowski, R. Jakiela, B. Lucznik, P. Kwiatkowski, M. Iwinska, M. Turek, H. Sakurai, T. Kachi, and M. Bockowski, Electronics **9**, 1380 (2020).
14) K. Sumida, K. Hirukawa, H. Sakurai, K. Sierakowski, M. Horita, M. Bockowski, T. Kachi, and J. Suda, Appl. Phys. Express **14**, 121004 (2021).
15) K. Hirukawa, K. Sumida, H. Sakurai, H. Fujikura, M. Horita, Y. Otoki, K. Sierakowski, M. Bockowski, T. Kachi, and J. Suda, Appl. Phys. Express **14**, 056501 (2021).
16) Ammono-GaN wafers sales, (http://ammono.com/index.php/ammono-gan-wafers-sales).
17) S. Rathkanthiwar, P. Bagheri, D. Khachariya, S. Mita, S. Pavlidis, P. Reddy, R. Kirste, J. Tweedie, Z. Sitar, and R. Collazo, Appl. Phys. Express **15**, 051003 (2022).
18) D. Khachariya, D. Szymanski, R. Sengupta, P. Reddy, E. Kohn, Z. Sitar, R. Collazo, and S. Pavlidis, J. Appl. Phys. **128**, 064501 (2020).
19) B. J. Baliga, *Advanced Power Rectifier Concepts* (Springer, Berlin, 2009).
20) B. J. Baliga, *Gallium Nitride and Silicon Carbide Power Devices* (World Scientific, Singapore, 2016), https://doi.org/10.1142/10027.
21) A. D. Koehler, T. J. Anderson, M. J. Tadjer, A. Nath, B. N. Feigelson, D. I. Shahin, K. D. Hobart, and F. J. Kub, ECS J. Solid State Sci. Technol. **6**, Q10 (2017).
22) F. Dahlquist, J. O. Svedberg, C.-M. Zetterling, M. Östling, B. Breitholtz, and H. Lendenmann, Mater. Sci. Forum **338–342**, 1179 (2000).
23) W. J. Sung, K. J. Han, and B. J. Baliga, Mater. Sci. Forum **924**, 613 (2018).
24) D. Khachariya, Ph.D. Thesis North Carolina State University (2021), (https://www.lib.ncsu.edu/resolver/1840.20/39175).
25) Y. Saitoh, K. Sumiyoshi, M. Okada, T. Horii, T. Miyazaki, H. Shiomi, M. Ueno, K. Katayama, M. Kiyama, and T. Nakamura, Appl. Phys. Express **3**, 081001 (2010).
26) Y. Zhang, M. Sun, Z. Liu, D. Piedra, M. Pan, X. Gao, Y. Lin, A. Zubair, L. Yu, and T. Palacios, 2016 IEEE Int. Electron Devices Meeting (IEDM), 2016, p. 10.2.1.
27) W. Li, K. Nomoto, M. Pilla, M. Pan, X. Gao, D. Jena, and H. G. Xing, IEEE Trans. Electron Devices **64**, 1635 (2017).
28) S. Han, S. Yang, and K. Sheng, IEEE Electron Device Lett. **40**, 1040 (2019).
29) X. Liu, Q. Liu, C. Li, J. Wang, W. Yu, K. Xu, and J.-P. Ao, Jpn. J. Appl. Phys. **56**, 026501 (2017).
30) Y. Cao, R. Chu, R. Li, M. Chen, and A. J. Williams, Appl. Phys. Lett. **108**, 112101 (2016).
31) T. Hayashida, T. Nanjo, A. Furukawa, and M. Yamamuka, Appl. Phys. Express **10**, 061003 (2017).
32) K. Hasegawa, G. Nishio, K. Yasunishi, N. Tanaka, N. Murakami, and T. Oka, Appl. Phys. Express **10**, 121002 (2017).
33) A. T. Binder et al., 2021 IEEE 8th Workshop on Wide Bandgap Power Devices and Applications (WiPDA), 2021, p. 288.